Bima Journal of Science and Technology, Vol. 8(3) Sept, 2024 ISSN: 2536-6041

DOI: 10.56892/bima.v8i3A.809

Enhanced Optical Response of Alumino-borophosphate Glasses Embedded with Gold Nanoparticles for Photonic Application

Ibrahim Mohammed Danmallam[1&2]*, Kabir Ahmed Dabai[1&3], Saeed Saad[1] Suleiman Bashir Adamu[4] and Ibrahim Bulus[5]

[1]Sokoto Energy Research Centre, Usmanu Danfodiyo University, Sokoto, Nigeria.
[2]Department of Physics, Faculty of Physical and Computing Science, Usmanu Danfodiyo University, Sokoto, Nigeria.
[3]Department of Electrical and Electronics Engineering, Faculty of Engineering and Environmental Design, Usmanu Danfodiyo University Sokoto, Nigeria.
[4]Department of Physics, Faculty of Natural and Applied Sciences, Sule Lamido University, 048 Kafin Hausa. Jigawa State, Nigeria.
[5]Department of Physics, School of Sciences, Kaduna State College of Education Gidan waya, Kafanchan, Nigeria.

Corresponding Author: ibrahimdanmallam@gmail.com

ABSTRACT

The demand for efficient, energy-saving, and environmentally friendly lighting devices remains a critical pursuit in materials science. In response to this need, we have developed a novel series of gold nanoparticles embedded in alumino-borophosphate glasses, using the conventional melt quenching technique. These glasses were subjected to both experimental and theoretical analyses to evaluate their potential for lasing and light-emitting applications. X-ray diffraction (XRD) confirmed the amorphous structure of the glass, while high-resolution transmission electron microscopy (HRTEM) images revealed spherical gold nanoparticles, averaging 15.01 nm in size, embedded within the glass matrix. The experimental absorption and photoluminescence spectra were further validated through Judd–Ofelt intensity and radiative parameter calculations. Notably, the incorporation of gold nanoparticles significantly enhanced the optical properties of the glass. In particular, the glass sample containing 0.7 mol% of gold nanoparticles exhibited a high branching ratio (72%), stimulated emission cross-section (30.24 × 10-20 cm^2), quantum efficiency (95%), and exceptional color purity (89%). The strong optical response achieved in this study underscores the suitability of these fabricated glasses for the development of an innovative solid-state red laser operating at 611 nm.

Keywords: Alumino-borophosphate glasses; Gold nanoparticles; Optical properties; Judd Ofelt parameters.

INTRODUCTION

The promising features of this glass host, which allows for tailoring the spectroscopic properties of rare earth-doped boro-phosphate glasses through surface plasmon resonance (SPR) by embedding metallic nanoparticles (NPs), present a challenging task. Achieving an optimal concentration of NPs is crucial for enhancing the optical response, making this approach valuable for photonic applications [1]. Equally, luminescence quenching of rare earth ions is detrimental for fabricating efficient lasers [2-3]. This drawback needs to be overcome, and significant enhancement of spectral features is essential [4-6]. Embedding metallic NPs/ or co-doping by low concentration of rare earth ions have proven to be alternative way to prevail such shortcomings [7-9]. Keeping in view of the

DOI: 10.56892/bima.v8i3A.809

significant and potential advantages of metallic nanoparticles embedded rare earth co-doped glass materials, the proposed research aims to investigate the influence of gold (Au) NPs on the optical response of Nd^{3+}/Er^{3+} Co-doped Alumino boro-phosphate glasses [10-11]. Based on the absorption and emission spectra, the spectroscopic properties such as spontaneous radiative emission probability (A_T), radiative lifetime (τ_R), luminescence branching ratio (β_R), effective bandwidth ($\Delta\lambda_{eff}$), stimulated emission cross section (σ_p), gain bandwidth ($\sigma_p \times \Delta\lambda_{eff}$), and optical gain ($\sigma_p \times \tau_R$) of Au NPs embedded Nd^{3+}/Er^{3+} Co-doped alumino-borophosphate glasses will be evaluated using Judd–Ofelt theory to ascertain their utility for solid state laser and light emitting devices [6-12]. Although numerous studies have explored phosphate glass systems, no definitive conclusions have been reached regarding the optimal composition or the ideal combination of nanoparticles and rare earth ions in these glasses. In this context, our findings may offer valuable insights toward the development of high-performance phosphate glass-based solid-state laser media, which are essential for a range of functional applications [13-14].

MATERIALS AND METHODS

Glass Sample Synthesis and Characterization

In this study, glasses were successfully synthesized using the conventional melt quenching technique. A 15-gram mixture was combined in a platinum crucible and subsequently melted at 900°C for 40 minutes. All raw materials were sourced from Sigma Aldrich Company. Once a suitable viscous mixture was achieved, the melt was annealed at 300°C for 3 hours by quenching it onto a stainless-steel mold. The furnace was then gradually cooled down to room temperature. The glass samples produced were visually transparent. They were characterized both thermally and optically using conventional spectroscopic techniques. Absorption analysis was carried out at room temperature using a monochromatic (Monk-Gillieson) spectrophotometer fitted with a photodiode detector, covering a wavelength range of 220 to 2600 nm. To ascertain the phase nature of the glass samples, X-ray diffraction (XRD) patterns were acquired employing a Siemens D5000 X-ray diffractometer.

RESULTS AND DISCUSSION

3.1 Physical and Optical properties of the glasses

Table 1 presents the physical and optical properties of the glasses, including density, molar volume, ionic concentration, polar radius, and molar refractivity. Figure 1(a) depicts the absorbance versus wavelength for the glasses in the UV-visible and near-infrared (NIR) regions, recorded over a wavelength range of 350 to 2240 nm, while Figure 1(b) shows the density and molar volume of the prepared glass system. As seen in Figure 1(a), there are approximately seven prominent absorption peaks across the ultraviolet-visible to near-infrared spectrum. The identified transitions in the ultraviolet (UV) region include $^7F_0 \rightarrow {}^5D_4$ (360 nm), $^7F_0 \rightarrow {}^5G_4$ (379 nm), $^7F_0 \rightarrow {}^5L_6$ (394 nm), $^7F_1 \rightarrow {}^5D_3$ (414 nm), $^7F_0 \rightarrow {}^5D_2$ (464 nm), $^7F_1 \rightarrow {}^5D_1$ (532 nm). Additionally, the NIR region shows transitions at $^7F_0 \rightarrow {}^5F_6$ (2090 nm), and $^7F_1 \rightarrow {}^5F_6$ (2205 nm). These transitions align with those reported in the literature [9,10].

Bima Journal of Science and Technology, Vol. 8(3) Sept, 2024 ISSN: 2536-6041

DOI: 10.56892/bima.v8i3A.809

Table 1: Physical and optical properties Au glasses

Parameters	Au-0.0	Au-0.2	Au-0.5	Au-0.8	Au-1.0
ρ (g/cm^3)	2.560	2.603	2.625	2.635	2.789
V_m (cm^3/mol)	54.22	50.47	49.96	49.69	46.87
$N \times 10^{22}$ (ions cm^{-3})	0.664	0.556	1.220	1.831	2.573
R_p (Å)	4.320	2.312	1.781	1.564	1.396
F ($\times 10^{16}$ cm^{-2})	7.258	11.84	19.89	26.01	32.63
R_i ($\times 10^{-23}$Å)	7.010	6.670	5.151	4.501	4.020
R %	0.991	1.371	1.411	1.503	1.542
R_M	46.11	30.02	27.57	27.23	26.91
α_e ($\times 10^{-23}$)	16.33	11.93	11.14	10.92	10.61

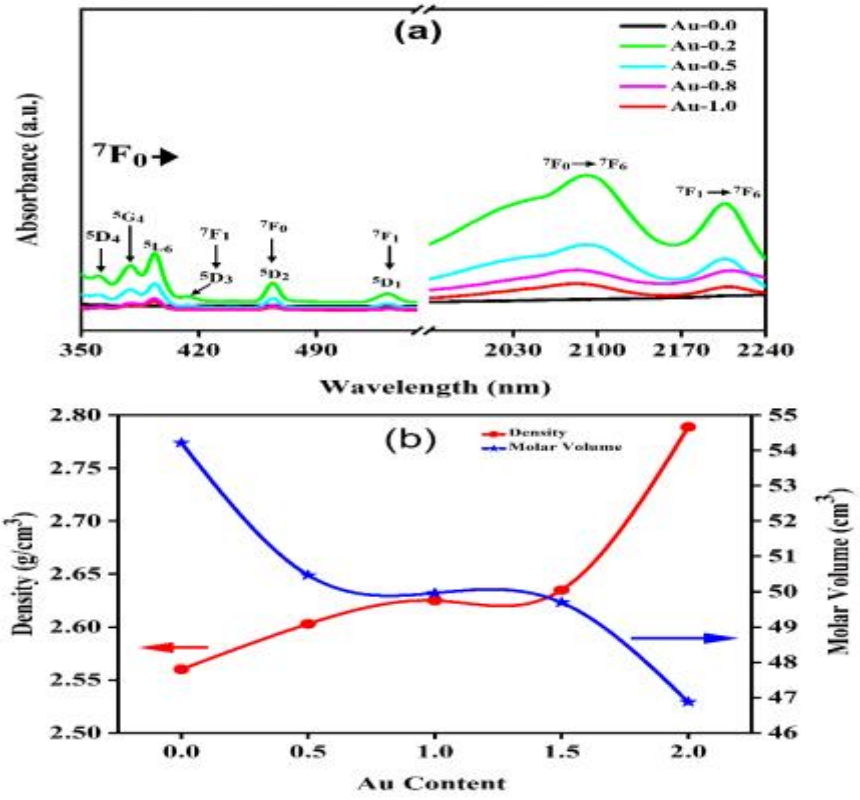

Figure 1: (a) Absorbance as function of wavelength and (b) density and molar volume of the prepared glass system

Structural properties

X-rays diffraction and Morphological structure

The XRD analysis shows no sharp peaks, indicating that the samples are amorphous and possess short-range order, as evidenced by a broad hump between 20° and 25° (2θ) in Figure 2. The absence of distinct crystalline peaks, combined with the broad hump, confirms the amorphous structure of the samples [10]. In addition, the low-resolution TEM image in Figure 3(a) clearly reveals gold nanoparticles (AuNPs) as dark spots. Figure 3(b) provides an HRTEM image along with a Fast Fourier Transform (FFT) diagram, highlighting the lattice fringes of the crystalline structure of the AuNPs. Notably, only the gold nanoparticles are visible,

DOI: 10.56892/bima.v8i3A.809

consistent with earlier studies [15-17]. The lattice fringes of the AuNPs are typically well-defined [18-19]. Furthermore, the TEM image of the selected Au-0.3 glass (Figure 3c) displays a uniform distribution of nearly spherical nanoparticles within the glass matrix, with an average diameter of approximately 27.65 nm, as shown in Figure 3(d).

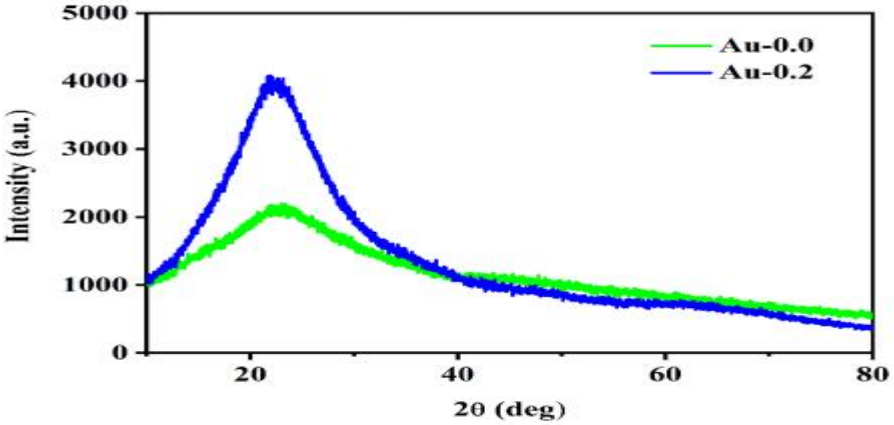

Figure 2: X-rays diffraction of the prepared glass system.

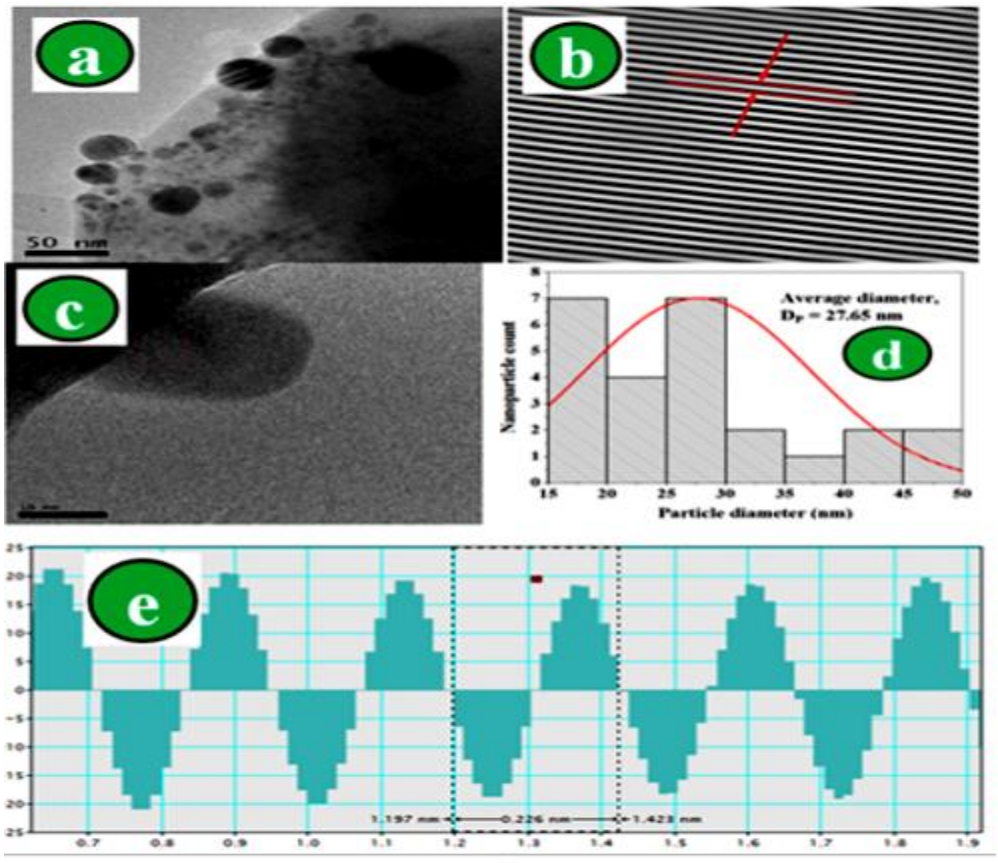

Figure 3: (a) HRTEM micrograph images of spherical AuNPs at different grid location (b) a single AuNPs with lattice fringes, (c) HRTEM image of a single AuNPs (d) average diameter of AuNPs of Au0.50 glass system

DOI: 10.56892/bima.v8i3A.809

Theoretical Analysis

Judd-Ofelt analysis

The Judd-Ofelt intensity parameter is an effective tool for analyzing the spectroscopic properties of materials, utilizing either absorption or emission spectra. For certain materials, however, emission spectra are necessary due to the lack of specific transitions [20,21]. The simulated emission cross-section is crucial for understanding lasing transitions. A higher Ω_2 value indicates greater asymmetry in rare earth ions and ligand field effects, while Ω_4 is influenced by transitional ions, the material's bulk properties, and its rigidity. The absence of the $^5D_0 \rightarrow {}^7F_6$ transition results in Ω6 to be zero [9, 21]. The Ω_λ value is derived from the intensity ratios of transitions and is given by

$$\Omega_\lambda = \frac{A_{ed}}{A_{ed}} \left\{ \frac{S_{md}\, \nu_1^3}{e^2\, \nu_\lambda^3} \right\} \left\{ \frac{9n^2}{(n^2+2)^2} \right\} \left[\left| \langle \psi J \| U^\lambda \| \psi' J' \rangle \right|^2 \right]^{-1}, \quad (1)$$

where n is refractive index, S_{md} is magnetic dipole, A_{ed} and A_{md} are electric and magnetic dipole transition probabilities and v_λ are transitions wavenumber.

The calculated data of the Judd-Ofelt intensity parameters and others related works are summarized in Table 3. The Au-0.5 glass demonstrates a high value of Ω_2 7.55×10^{-20}cm^2. Conversely, the Au-0.8 glass displays the lowest value of Ω_2 at 6.21×10^{-20}cm^2 as concentration of AuNPs increases from 0.5 to 1.0g.

Table 2: Calculated data of Judd-Ofelt parameters of the studied glasses and other related works.

Glass code	Ω_2	Ω_4	Ω_6	Trend	Reference
Au-0.0	6.41	2.70	0	$\Omega_2 > \Omega_4 > \Omega_6$	This study
Au-0.2	6.88	2.36	0	$\Omega_2 > \Omega_4 > \Omega_6$	This study
Au-0.5	7.55	2.42	0	$\Omega_2 > \Omega_4 > \Omega_6$	This study
Au-0.8	6.21	2.05	0	$\Omega_2 > \Omega_4 > \Omega_6$	This study
Au-1.0	7.45	2.06	0	$\Omega_2 > \Omega_4 > \Omega_6$	This study
TBZEu0.03	3.37	1.82	0	$\Omega_2 > \Omega_4 > \Omega_6$	[9]
PKMNC	5.62	2.05	0	$\Omega_2 > \Omega_4 > \Omega_6$	[22]
CSEu0.1	3.55	0	0	$\Omega_2 > \Omega_4 > \Omega_6$	[23]
BGG	5.45	4.45	0	$\Omega_2 > \Omega_4 > \Omega_6$	[24]

*[9]Borotellurite, *[22]Phosphate, *[23]Calcium silicate, *[24]Borogermanate.

Table 3. Radiative parameter, branching ratio and stimulated emission cross-section of $^5D_0 \rightarrow {}^7F_2$ transition of studied glasses and others related studies.

Glass code	A_{rad}, s^{-1}	β_r, %	σ_{em},($\times10^{-22}$cm^2)	Reference
Au-0.2	375.00	61.6	9.55	This study
BPEu0.25	125.49	61.0	10.05	[16]
PAZE20	219.00	71.0	8.36	[17]
TBZEu0.03	565.10	61.1	12.57	[9]
TZNSAu-4	357.00	37	0.143	[25]
TZNSAu-3	294.00	45	0.273	[25]
BTBaEu0.05	150.00	69	17.5	[26]

*[16]Borophosphate, *[17]Sodium phosphate, *[9]Borotellurite, *[25]Sodium zinc-tellurite, *[26]Barium-telluraborate

DOI: 10.56892/bima.v8i3A.809

Radiative parameters

The critical parameters, such as the stimulated emission cross-section, are essential in evaluating the optical excellence of the glass for potential laser applications. A branching ratio exceeding 50% is necessary for lasing, which is achieved in all $^5D_0 \rightarrow {}^7F_2$ transitions. The Au-0.2 glass exhibits the highest values for emission cross-section, optical gain, and gain bandwidth [27]. The electric dipole transition probability (A_{ed}) is given by equation (2)

$$A_{ed} = \left[\frac{64\pi^4 v^3 \, n(n^2+2)^2}{27\hbar(2J+1)}\right] S_{ed} \qquad (2)$$

where in equation (2). The branching ratio (β_r) is the radiative transition probability ratio to sum of radiative transition in all levels. Meanwhile, τ_{cal} is defined as a calculated lifetime associated with the sum of all radiative transition. The branching ratio and τ_{cal} are given as expressed as follows:

$$\beta_r = \frac{A_{rad}}{\sum A_{rad}} \qquad (3)$$

$$\tau_{cal} = \frac{1}{\sum A_{rad}} \qquad (5)$$

Furthermore, emission cross-section is given by

$$A_e = \frac{\lambda P^4}{8\pi c n^2 \Delta_{eff}} A(\psi j) \qquad (6)$$

where λp emission peak, *n* is the refractive index, and c is the speed of light in vacuum.

Table 4 presents the transition probabilities (A_{rad}), branching ratios (β_r), emission cross-section of the excited state, optical bandwidth, and optical gain width for the $^5D_0 \rightarrow {}^7F_2$ transitions of the co-embedded nanoparticles [15,28]. The importance of the branching ratio in laser development highlights the need for higher stimulated emission values in glass transitions [9]. The trend in intensity parameters suggests structural changes in the surrounding rare earth ions, indicating a dominance of short-range influences and covalent characteristics, while Ω_4 is associated with bulk properties such as rigidity and viscosity [9,15]. A higher intensity of Ω_2 supports the hypersensitive transition $^5D_0 \rightarrow {}^7F_2$, indicating that europium ions are situated in a polarizable chemical environment [9, 29-31].

Decay curve, quantum efficiency and CIE chromaticity analysis

The experimental decay time (τexp) is described by the equation $I = I_0 \exp(-t/\tau)$. The measured decay times (τexp = 1335.1, 1773, 2044.9 μs) are shorter than the calculated radiative lifetimes (τcal = 1558, 1895.5, 2000.1 μs). This discrepancy arises from the differences in radiative and non-radiative decay rates. The quantum efficiency (η) of the corresponding levels is calculated as the ratio of the experimental lifetime to the evaluated lifetime, expressed as a percentage: 93.5%, 85.7%, and 97.9%, respectively. Figure 4 depicts the calculated CIE chromaticity coordinates for the synthesized glasses, with values falling within the NTSC threshold for

DOI: 10.56892/bima.v8i3A.809

red phosphor (x = 0.67, y = 0.33). This suggests the glasses' as ideal candidate for red laser applications.

Table 4. The radiative properties of the synthesized glasses

Transition	Parameters and units	Au-0.0	Au-0.2	Au-0.5	Au-0.8	Au-1.0
$^5D_0 \rightarrow {}^7F_1$	$\lambda_{p,}$ nm	592	590	591	591	592
	$A_{rad,}$ s^{-1}	180	180	182	183	183
	$\beta_{r,}$ %	32.19	30.9	29.5	33.6	30.1
	σ, ($\times 10^{-22} cm^2$)	3.067	4.047	4.23	3.78	3.1
	$\sigma \times$FWHM ($\times 10^{-20} cm^2$)	0.611	0.610	0.610	0.610	0.617
	$\sigma \times \tau_{cal}$ ($\times 10^{-25}$ $cm^2 s^{-1}$)	5.431	6.87	6.85	6.94	5.1
$^5D_0 \rightarrow {}^7F_2$	$\lambda_{p,}$ nm	614	613	614	614	614
	$A_{rad,}$ s^{-1}	319	350	377	311	375
	$\beta_{r,}$ %	56.4	59.4	61	57.2	61.6
	$\sigma(\times 10^{-22} cm^2)$	8.113	7.465	8.48	6.35	9.55
	$\sigma \times$FWHM ($\times 10^{-20} cm^2$)	1.245	1.33	1.47	1.22	1.47
	$\sigma \times \tau_{cal}$ ($\times 10^{-25}$ $cm^2 s^{-1}$)	14.367	12.7	13.7	11.7	15.7
$^5D_0 \rightarrow {}^7F_4$	$\lambda_{p,}$ nm	700	699	700	700	699
	$A_{rad,}$ s^{-1}	65.094	56.9	58.6	49.7	50.2
	$\beta_{r,}$ %	11.5	9.65	9.49	9.16	8.27
	$\sigma(\times 10^{-22} cm^2)$	3.104	3.06	3.28	2.76	2.39
	$\sigma \times$FWHM ($\times 10^{-20} cm^2$)	0.430	0.374	0.388	0.329	0.323
	$\sigma \times \tau_{cal}$ ($\times 10^{-25}$ $cm^2 s^{-1}$)	5.497	5.19	5.31	5.07	3.94
	$A_{T,}$ s^{-1}	564.68	588.9	617.6	543.7	608.2
	$\tau_{cal,}$ ms	1.771	1.698	1.619	1.839	1.644

DOI: 10.56892/bima.v8i3A.809

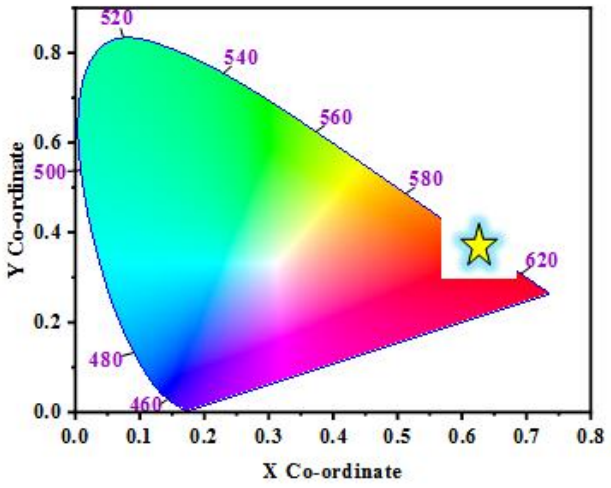

Figure 3: The CIE chromaticity diagram of the synthesized glasses.

CONCLUSION

In this study, the impact of co-embedded Gold (Au) nanoparticles on alumino-borophosphate has been explored by focusing on Judd-Ofelt parameters and the radiative properties of Eu^{3+} ions. A consistent trend of $\Omega_2 > \Omega_4 > \Omega_6$ was observed across all the glasses studied, with values ranging from 2.05×10^{-20} cm² to 7.55×10^{-20} cm^2. Radiative parameters, including emission cross-section and branching ratio, were evaluated, with the $^5D_0 \rightarrow {}^7F_2$ transition showing the highest branching ratio at 61.6%. This exceptional radiative emission observed suggest that these glasses are highly suitable as active media for red lasers. HRTEM analysis confirmed the presence of AuNPs with an average size of 27.65 nm. The core-shell structure of the bimetallic nanoparticles provides superior optical properties compared to monometallic nanoparticles, making them ideal for optically driven applications. The large, stimulated emission cross-section achieved highlights the potential of these materials for use in photonic devices and as active media for visible red lasers. The synthesized Au-0.30 glass sample demonstrated a high quantum efficiency (η = 97.9%), significantly enhancing the photoluminescence intensity of the red peak, making it an excellent candidate for red laser applications.

Acknowledgments

The authors are grateful Grant name. TETFUND Institutional Based Research (IBR) Grant Usmanu Danfodiyo University Sokoto. Batch 8.

REFERENCES

[1] I. Abdullahi, S. Hashim, S.K. Ghoshal, Waveguide laser potency of samarium doped $BaSO_4$-TeO_2-B_2O_3 glasses: Evaluation of structural and optical qualities, J. Lumin. 216 (2019) 116686.

[2] H. Zhang, J. Okuni, N. Toshima, One-pot synthesis of Ag-Au bimetallic nanoparticles with Au shell and their high catalytic activity for aerobic glucose oxidation, J. Colloid Interface Sci. 354 (2011) 131–138.

[3] Y. Wu, X. Xu, X. Yu, B. Zhang, Q. Li, J. Qiu, Improved photoluminescence behavior of Eu^{3+} activated $Ca_5(PO_4$ F red nanophosphor by adding Li+, Au^{3+} , and Bi^{3+} $)_3$ as co-dopants, Chinese Opt. Lett. 12 (2014) 10–13.

[4] G. Seifert, A. Stalmashonak, H. Hofmeister, J. Haug, M. Dubiel, Laser-induced, polarization dependent shape transformation of Au/Ag nanoparticles in glass, Nanoscale Res. Lett. 4 (2009) 1380–1383.

[5] I.M. Danmallam, S.K. Ghoshal, R. Ariffin, S.A. Jupri, S. Sharma, Europium ions and silver nanoparticles co-doped magnesium-zinc-sulfophosphate glasses: Evaluation of ligand field and Judd-Ofelt parameters, J. Lumin. (2019) 116713.

[6] M.G. Ventura, A.J. Parola, A.P. De Matos, Influence of heat treatment on the colour of Au and Ag glasses produced by the sol-gel pathway, J. Non. Cryst. Solids.

DOI: 10.56892/bima.v8i3A.809

357 (2011) 1342–1349.

[7] A.S. Alqarni, R. Hussin, S.K. Ghoshal, S.N. Alamri, Y.A. Yamusa, S.A. Jupri, Intense red and green luminescence from holmium activated zinc-sulfo-boro-phosphate glass: Judd-Ofelt evaluation, J. Alloys Compd. 808 (2019) 151706.

[8] R. Ma, J. Gao, Q. Xu, S. Cui, X. Qiao, J. Du, X. Fan, Eu^{2+} promoted formation of molecule-like Ag and enhanced white luminescence of Ag/Eu-codoped oxyfluoride glasses, J. Non. Cryst. Solids. 432 (2016) 348–353.

[9] Adamu, S. B., Halimah, M. K., Chan, K. T., Muhammad, F. D., Nazrin, S. N., & Tafida, R. A. (2022). Eu^{3+} ions doped zinc borotellurite glass system for white light laser application: Structural, physical, optical properties, and Judd-Ofelt theory. Journal of Luminescence, 250, 119099.

[10] T. Som, B. Karmakar, Core-shell Au-Ag nanoparticles in dielectric nanocomposites with plasmon-enhanced fluorescence: A new paradigm in antimony glasses, Nano Res. 2 (2009) 607–616.

[11] H. Xia, J. Zhang, J. Wang, Y. Zhang, Haiping Xia, Jianli Zhang et al., The optical spectra and local structure of Eu^{3+} ion doped in Nb2O5-La2O3-B2O3-BaO glasses. Chin. Opt. Lett. 4, 476-479, 2006., Chinese Opt. Lett. 4 (2006) 476–479.

[12] R. Vijayakumar, K. Marimuthu, Luminescence studies on Ag nanoparticles embedded Eu^{3+} doped boro-phosphate glasses, J. Alloys Compd. 665 (2016) 294–303.

[13] M. Shwetha, B. Eraiah, Influence of europium (Eu^{3+}) ions on the optical properties of lithium zinc phosphate glasses, IOP Conf. Ser. Mater. Sci. Eng. 310 (2018).

[14] K. Linganna, C.K. Jayasankar, Optical properties of Eu^{3+} ions in phosphate glasses, Spectrochim. Acta - Part A Mol. Biomol. Spectrosc. 97 (2012) 788–797.

[15] Q. Jiao, J. Qiu, D. Zhou, X. Xu, Contribution of Eu ions on the precipitation of silver nanoparticles in Ag-Eu co-doped borate glasses, Mater. Res. Bull. 51 (2014) 315–319.

[16] L.R.P. Kassab, D.S. Silva, C.B. De Araújo, L.R.P. Kassab, D.S. Silva, C.B. De Araújo, Influence of metallic nanoparticles on electric-dipole and magnetic-dipole transitions of Eu^{3+} doped germanate glasses, J. Appl. Phys. 113506 (2014) 3–8.

[17] M. Saad, W. Stambouli, S.A. Mohamed, H. Elhouichet, Ag nanoparticles induced luminescence enhancement of Eu^{3+} doped phosphate glasses, J. Alloys Compd. 705 (2017) 550–558.

[18] I.M. Danmallam, S. Krishna, R. Ariffin, S. Aisha, Controlled physical and optical traits of magnesium-zinc sulphophosphate glass : role of europium ions, Malaysian J. Fundam. Appl. Sci. 222 (2018) 78–82.

[19] M.A. Garcia, Surface plasmons in metallic nanoparticles: Fundamentals and applications, J. Phys. D. Appl. Phys. 44 (2011).

[20] X. Hu, Q. Zhao, X. Jiang, C. Zhu, J. Qiu, Space-selective co-precipitation of silver and gold nanoparticles in femtosecond laser pulses irradiated Ag^{+}, Au^{3+} co-doped silicate glass, Solid State Commun. 138 (2006) 43–46.

[21] H. Yu, Effects of charge compensation on red emission in, Chinese Opt. Lett. 12 (2014) 10–13.

[22] C. Srinivasa Rao, K. Upendra Kumar, C.K. Jayasankar, Luminescence properties of Eu^{3+} ions in phosphate-based bioactive glasses, Solid State Sci. 13 (2011) 1309–1314.

[23] R.A. Barve, N. Suriyamurthy, B.S.

DOI: 10.56892/bima.v8i3A.809

Panigrahi, B. Venkatraman, Optical properties and Judd–Ofelt analysis of Eu^{3+} activated calcium silicate, Phys. B Condens. Matter. 475 (2015) 156–161.

[24] M. Gökçe, U. Şentürk, D.K. Uslu, G. Burgaz, Y. Şahin, A. Gürhan Gökçe, Investigation of europium concentration dependence on the luminescent properties of borogermanate glasses, J. Lumin. 192 (2017) 263–268.

[25] A. Ćirić, S. Stojadinović, M.D. Dramićanin, Judd-Ofelt and chromaticity analysis of hafnia doped with trivalent europium as a potential white LED phosphor, Opt. Mater. (Amst). 88 (2019) 392–395.

[26] S.Q. Mawlud, A comparative enhancement of Au and Ag NPs role on radiative properties in Sm^{3+} doped zinc-sodium tellurite glass: Judd-Ofelt parameter, Spectrochim. Acta-Part A Mol. Biomol. Spectrosc. 209 (2019) 78–84.

[27] K. Annapoorani, K. Marimuthu, Spectroscopic properties of Eu^{3+} ions doped Barium telluroborate glasses for red laser applications, J. Non. Cryst. Solids. 463 (2017) 148–157.

[28] K.K. Rasu, D. Balaji, S.M. Babu, Spectroscopic properties of Eu^{3+}:$KLa(WO_4)_2$ novel red phosphors, J. Lumin. 170 (2016) 547–555.

[29] M. Reza Dousti, M.R. Sahar, M.S. Rohani, A. Samavati, Z.A. Mahraz, R.J. Amjad, A. Awang, R. Arifin, Nano-silver enhanced luminescence of Eu^{3+} doped lead tellurite glass, J. Mol. Struct. 1065–1066 (2014) 39–42.

[30] I.M. Danmallam, S.K. Ghoshal, R. Ariffin, S.A. Jupri, S. Sharma, I. Bulus, Judd-Ofelt evaluation of europium ion transition enhancement in phosphate glass, Optik (Stuttg). 196 (2019) 163197.

[31] C.R. Kesavulu, K.K. Kumar, N. Vijaya, K.S. Lim, C.K. Jayasankar, Thermal, vibrational and optical properties of Eu^{3+} doped lead fluorophosphate glasses for red laser applications, Mater. Chem. Phys. 141 (2013) 903–911.